Temporal Relations of Column Water Vapor and Tropical Precipitation

CHRISTOPHER E. HOLLOWAY*

Department of Atmospheric and Oceanic Sciences, University of California, Los Angeles, Los Angeles, California

J. DAVID NEELIN

Department of Atmospheric and Oceanic Sciences, and Institute of Geophysics and Planetary Physics, University of California, Los Angeles, Los Angeles, California

(Manuscript received 7 August 2009, in final form 9 November 2009)

ABSTRACT

Empirical studies using satellite data and radiosondes have shown that precipitation increases with column water vapor (CWV) in the tropics, and that this increase is much steeper above some critical CWV value. Here, eight years of 1-min-resolution microwave radiometer and optical gauge data at Nauru Island are analyzed to better understand the relationships among CWV, column liquid water (CLW), and precipitation at small time scales. CWV is found to have large autocorrelation times compared with CLW and precipitation. Before precipitation events, CWV increases on both a synoptic-scale time period and a subsequent shorter time period consistent with mesoscale convective activity; the latter period is associated with the highest CWV levels. Probabilities of precipitation increase greatly with CWV. Given initial high CWV, this increased probability of precipitation persists at least 10–12 h. Even in periods of high CWV, however, probabilities of initial precipitation in a 5-min period remain low enough that there tends to be a lag before the start of the next precipitation event. This is consistent with precipitation occurring stochastically within environments containing high CWV, with the latter being established by a combination of synoptic-scale and mesoscale forcing.

1. Introduction

Observational studies have shown that increased lower-tropospheric moisture tends to lead deep convection and precipitation in the tropics (Sherwood 1999; Sherwood et al. 2004; Sobel et al. 2004; Mapes et al. 2006; Zelinka and Hartmann 2009; Mapes et al. 2009). Studies using cloud system–resolving models (CSRMs) have also found that deep convection is sensitive to lower-tropospheric moisture (Tompkins 2001; Grabowski 2003; Derbyshire et al. 2004). This has important implications for convective organization; for instance, several studies document lower-tropospheric moistening several days before an active phase of the Madden–Julian oscillation (MJO) in the Indo-Pacific warm pool (e.g., Maloney and Hartmann 1998; Kiladis et al. 2005). Bretherton et al. (2005) found that feedback among convection, tropospheric moisture, and radiation played a key role in convective self-aggregation in a CSRM radiative–convective equilibrium simulation.

Recent observational studies have also found an empirical relationship between tropical column water vapor (CWV) and precipitation (Bretherton et al. 2004; Peters and Neelin 2006; Neelin et al. 2009). However, the satellite data used in these studies are at twice-daily or coarser temporal resolution, and they do not attempt to analyze temporal relationships between different variables. Sherwood and Wahrlich (1999) used rawinsondes along with satellite data to show that CWV is high within 3 h of convective onset and then decreases during and after convection, but again they had fairly coarse temporal resolution.

Holloway and Neelin (2009) showed that high CWV corresponds to high precipitation at little or no lag using radiosonde and gauge data at Nauru. Furthermore, there

* Current affiliation: NCAS Centre for Global Atmospheric Modelling, Department of Meteorology, University of Reading, Reading, United Kingdom.

Corresponding author address: Christopher E. Holloway, Department of Meteorology, University of Reading, Earley Gate, P.O. Box 243, Reading RG6 6BB, United Kingdom.
E-mail: chollow@ucla.edu

DOI: 10.1175/2009JAS3284.1

is evidence that boundary layer and lower-tropospheric moisture can lead precipitation by an hour or two whereas middle- and upper-tropospheric moisture tends to lag precipitation by the same amount of time, in agreement with Sobel et al. (2004). Since Holloway and Neelin (2009) found that variance in CWV corresponds mainly to moisture variance in the lower free troposphere (peaking around 800 hPa), studies looking at temporal patterns of moisture at those levels should see behavior similar to that of CWV. Mapes et al. (2006) shows that moisture from roughly 700 to 800 hPa tends to increase several days before maximum rainfall and then decreases fairly rapidly afterward, although it is somewhat offset by increased moisture at higher levels after maximum rainfall.

Given that CWV has a much longer characteristic autocorrelation time scale than precipitation (Neelin et al. 2008), we explore the hypothesis proposed in previous studies that CWV (and therefore lower-free-tropospheric moisture) provides memory to the tropical atmosphere and can be a precursor to deep convection (e.g., Sherwood 1999). Since column moistening is more gradual than the onset of strong precipitation and often precedes it, other factors have been proposed to explain the behavior of lower-tropospheric moisture. One explanation proposed is that synoptic-scale waves cause moistening (Haertel and Kiladis 2004; Tian et al. 2006). As precipitation becomes more widespread as part of an organized mesoscale system, the two-way interaction between CWV and precipitation should become more important (e.g., Grabowski and Moncrieff 2004). Mechanisms proposed for moistening ahead of mesoscale convective systems include the gravity wave response to the first baroclinic mode of heating (Mapes 1993; Fovell et al. 2006). We use one well-instrumented observational site to add additional insight to these previous ideas.

Here we aim to substantiate and add nuance to the argument that CWV can be seen as a relatively slowly changing predictor variable that increases the probability of precipitation events, which have much shorter characteristic time scales. Holloway and Neelin (2009) showed that CWV variability is likely related to that of lower-tropospheric moisture, and that increased CWV therefore increases the buoyancy of entraining plumes, leading to an increased chance of deep convection. However, there are also positive feedbacks between deep convection and lower-tropospheric moisture. We ask the following: to what extent does CWV tend to increase over longer time scales without obvious interactions with precipitation until higher CWV values are reached, and to what extent do increases occur on mesoscale time scales when these feedbacks are likely to be more important?

We use 8 yr of microwave radiometer data, precipitation gauge data, and cloud height measurements from the ARM station at Nauru (section 2). These data are provided at 1-min resolution, allowing us to explore the relationship between CWV and precipitation at various lag times (from a few minutes to a few days). After comparing autocorrelation time scales and addressing some key interpolation issues in section 3, we investigate the pickup of precipitation with CWV at different time lags in section 4. In section 5 we show how CWV and column liquid water (CLW) composites evolve before and after strong precipitation events and around the transition from suppressed to normal precipitation. The dependence of the transition to high precipitation probabilities on CWV is further explored using conditional averaging in section 6 and composites on CWV increases in section 7. We present our conclusions in section 8.

2. Data and methodology

The Department of Energy's Atmospheric Radiation Measurement (ARM) program (Stokes and Schwartz 1994) maintains a climate observation site at Nauru Island (0.5°S, 166.9°E; Mather et al. 1998). We have analyzed microwave radiometer (MWR) CWV and column liquid water data as well as optical gauge surface precipitation rates from 20 November 1998 to 16 August 2006. The data are at 1-min temporal resolution. The precipitation rate has 0.1 mm h^{-1} resolution and 0.1 mm h^{-1} uncertainty.

The MWR instrument passively measures downward microwave radiation reaching the surface at 23.8 and 31.4 GHz. To remove version inconsistencies in the retrievals of CWV and CLW, we have reanalyzed the MWR brightness temperatures using the latest ARM algorithms based on Liljegren et al. (2005). These algorithms are weighted linear combinations of the optical depths of the two channels (which are derived from the brightness temperatures), with the weights determined by linear regression over a climatological range of conditions comeasured by radiosondes. The MWR instrument showed large agreement with high-quality radiosondes from the Japanese R/V *Mirai* during the Nauru99 campaign, with a maximum CWV difference of 3 mm (Westwater et al. 2003).

There is fairly good agreement between CWV from the MWR and that from the radiosondes analyzed in Holloway and Neelin (2009), with a correlation of 0.92, although at high CWV values the radiosondes tend to be moister (see section 3 below). This could have something to do with the wet window problem: the radiometer cannot function correctly when its window becomes moist. When this happens, a heater and fan turn on until the window dries. The data are flagged as missing until the heater and fan shut off and the window is dry. Because we are interested in CWV and CLW values near

precipitating times, we need to find a way to estimate these fields when the MWR window is wet. We have chosen to interpolate over gaps less than 12 h long for CWV and CLW values, and we identify these fields as ''gap-filled'' data hereafter (discussed further in section 3 below).

Cloud-top and cloud-bottom height data are taken over the whole period from the ARM Active Remotely Sensed Cloud Locations (ARSCL) product, which combines micropulse lidar and cloud radar measurements (Clothiaux et al. 2000), although there are large gaps of missing data from October 2000 to June 2001, from September 2002 to September 2003, and from January 2005 to August 2006. There are attenuation effects present at rainfall amounts above 5 mm h^{-1} (Jensen and Del Genio 2006).

3. Temporal autocorrelation scales and gap-filled data

Figure 1 shows that CWV has fairly long autocorrelation times compared with CLW and precipitation. The autocorrelation is still above 0.7 even at 24-h lag. This has a number of potential implications for the CWV–precipitation relationship, and we explore or make use of some of these implications in this study. These include links to mechanisms of mesoscale organization as well as the extent to which CWV might be used as a predictor of future precipitation (e.g., in stochastic parameterization).

In this study, there is a practical reason to utilize this long autocorrelation time in order to justify interpolating over gaps less than 12 h long caused by the wet window problem, which eliminates CWV and CLW measurements during and just after rainfall as discussed in section 2. This interpolation is harder to justify for CLW, which has relatively short autocorrelation scales, so we make very limited conclusions based on gap-filled values for CLW.

Figure 2 shows examples of five 5-day time series of CWV (black dots) with gray circles showing gaps filled by interpolation and blue open circles showing precipitation. These five series were chosen from 20 randomly selected periods and represent the main features and variability contained in those time series. It is clear that many CWV peaks are still cut off, meaning we are undersampling the highest values. One gap is even longer than 12 h and is not filled. Large gaps seem to be preferentially cut off before the peak, leading to interpolated lines that slope upward in time, which could affect some composites done in later sections. There are also some times, such as the first two days in the top panel of Fig. 2, when the interpolation is done over very small gaps, mainly because of temporary changes in instrument temporal resolution, which should not affect the results at all. The other gaps are all due to precipitation, with the wider gaps generally associated with stronger precipitation that lasts longer.

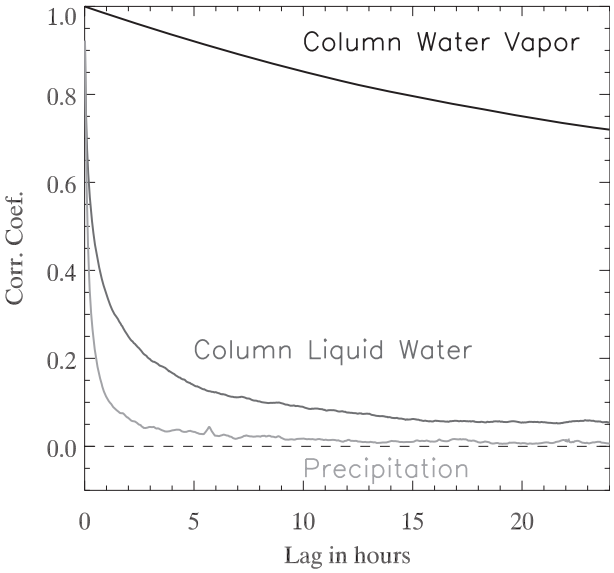

FIG. 1. Autocorrelation vs lag for column water vapor (black), column liquid water (dark gray), and precipitation (light gray), for all data.

Comparing histograms of gap-filled and non-gap-filled CWV, we can see from Fig. 3 that the higher bins tend to be disproportionately increased for gap-filled data. From Fig. 2 we can surmise that observations falling in the highest bins are being attributed to slightly lower bins in the gap-filled data, but this problem is not so severe as to create a spurious bump in the histogram.

We also compare the radiometer data to Nauru ARM radiosonde data, available between April 2001 and August 2006 (see Holloway and Neelin 2009), as well as to nearby Tropical Rainfall Measuring Mission (TRMM) Microwave Imager (TMI) satellite CWV data, centered at 0.625°S, 166.875°E, for those same years. The TMI data are at 0.25° × 0.25° resolution, from the Hilburn and Wentz (2008) algorithm. The radiometer data comparisons are done at the minute of each sonde launch and separately at the minute of TMI overpass. Figures 4a and 4b show that for the full interpolated MWR data there is fairly close agreement between the two datasets over most of the data range, although the radiometer data are about 1–2 mm higher than the sonde data for MWR bins between 55 and 60 mm and 2–3 mm higher than the TMI data for several MWR bins between 58 and 65 mm. The results are shown separately for conditional averages on each of the variables in each plot, along with the full scatterplot, to illustrate spurious trends due to binning in a single direction. The averages at the high end of the CWV values tend to diverge, so the

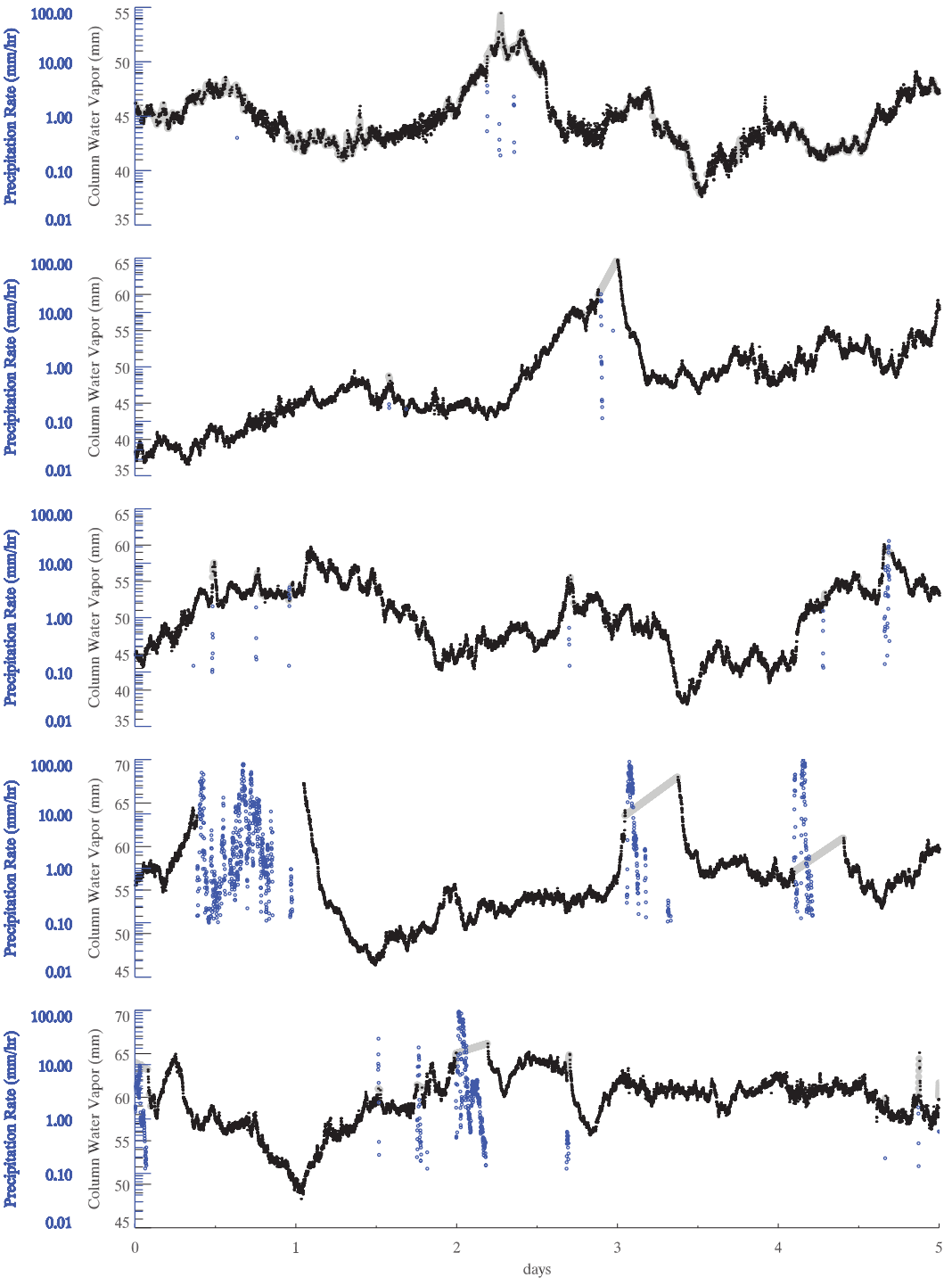

FIG. 2. Five example 5-day time series of CWV (black dots), showing filled gaps in gray. Blue open circles show precipitation (log scale).

discussion of bias should be based on the scatterplot at this end. The TMI comparison shows very good agreement even at the higher end (though there are fewer high TMI values), while a small number of high radiosonde values with much lower MWR values may indicate a few problematic radiosondes.

Looking at these comparisons only for the interpolated gaps (Figs. 4c,d), the radiometer again overestimates the

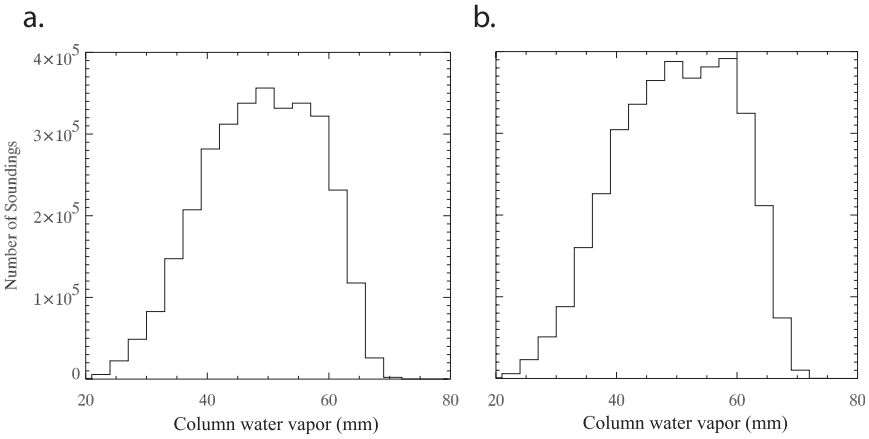

FIG. 3. Histograms of column water vapor values for (a) original data and (b) gap-filled data. Bins are 3 mm wide.

observed values for most bins, by up to around 3 mm. However, the scatterplot is mostly fairly close to the one-to-one line, and near the high end it appears to be closer than the non-gap-filled data. The full interpolated MWR data (Figs. 4e,f) do not look much different from the noninterpolated data, again showing that the interpolated gaps are not adding much extra bias, if any.

Gap-filled data are clearly superior to non-gap-filled data for the purposes of this study, since the gaps are not random, occurring preferentially at the most important part of the distribution and the most relevant parts of the time series—those surrounding precipitation and high CWV values. That said, when we reproduced the composites in the following sections using only the non-gap-filled data (not shown), we found the same main conclusions. The ambient mean values and overall curves were shifted about 1.5 (0.03) mm lower for CWV (CLW), and the overall curves in the composites outside times with especially strong or suppressed precipitation were also shifted similarly. In addition, the peaks within about ± 7 h of precipitation maxima in the composites on strong precipitation (where there are very few non-gap-filled data points) were less steep and were lower, reaching maxima about 2.5 (0.2) mm less than the interpolated data when measured against the ambient mean values for CWV (CLW). Curves at times with suppressed precipitation were virtually identical in both datasets since those times have very few gaps requiring interpolation.

4. Precipitation pickup as a function of lag

Even at 3-h lag and for non-gap-filled data, Fig. 5 shows that we can reproduce the pickup of precipitation at high CWV seen in earlier satellite-based studies (Bretherton et al. 2004; Peters and Neelin 2006) and in radiosondes at the same Nauru ARM site (Holloway and Neelin 2009). This lag is necessary here to avoid the wet window problem discussed above. There are proportionately few values of very high CWV available even for the gap-filled data as compared with the radiosonde data in Holloway and Neelin (2009), probably because of the wet window problem and the problems the MWR can have at high CLW values. This makes it impossible to test the power-law relationship at high CWV, as seen in Peters and Neelin (2006).

Figure 6 shows the CWV relationship to average precipitation rate (on log scale) at ± 12-h lags (measured in time after CWV measurement), using gap-filled data. There is certainly an increase of precipitation with CWV at all lags. Overall, there is a fairly symmetric pattern in time, although the center of the precipitation peak tends to occur about an hour before the high CWV measurement. On the other hand, there is more precipitation at long lags (6–12 h) after high CWV than there is for those same lead times. This suggests that the CWV–precipitation relationship is not simply due to rain moistening the air immediately around it, which would cause a reversed lag relationship.

5. Time composites on precipitation events

To investigate the average behavior of CWV around a precipitation event, we have made composites centered on locally high precipitation (above the median positive precipitation rate, 0.97 mm h^{-1}, and higher than neighboring events within the composite window). Figure 7 shows these composites for gap-filled CWV and CLW (see section 3), as well as for precipitation itself (the nonsmoothed peak at zero lag, inset at log scale, reaches 65 mm h^{-1}), for ± 48 h of a precipitation maximum (330

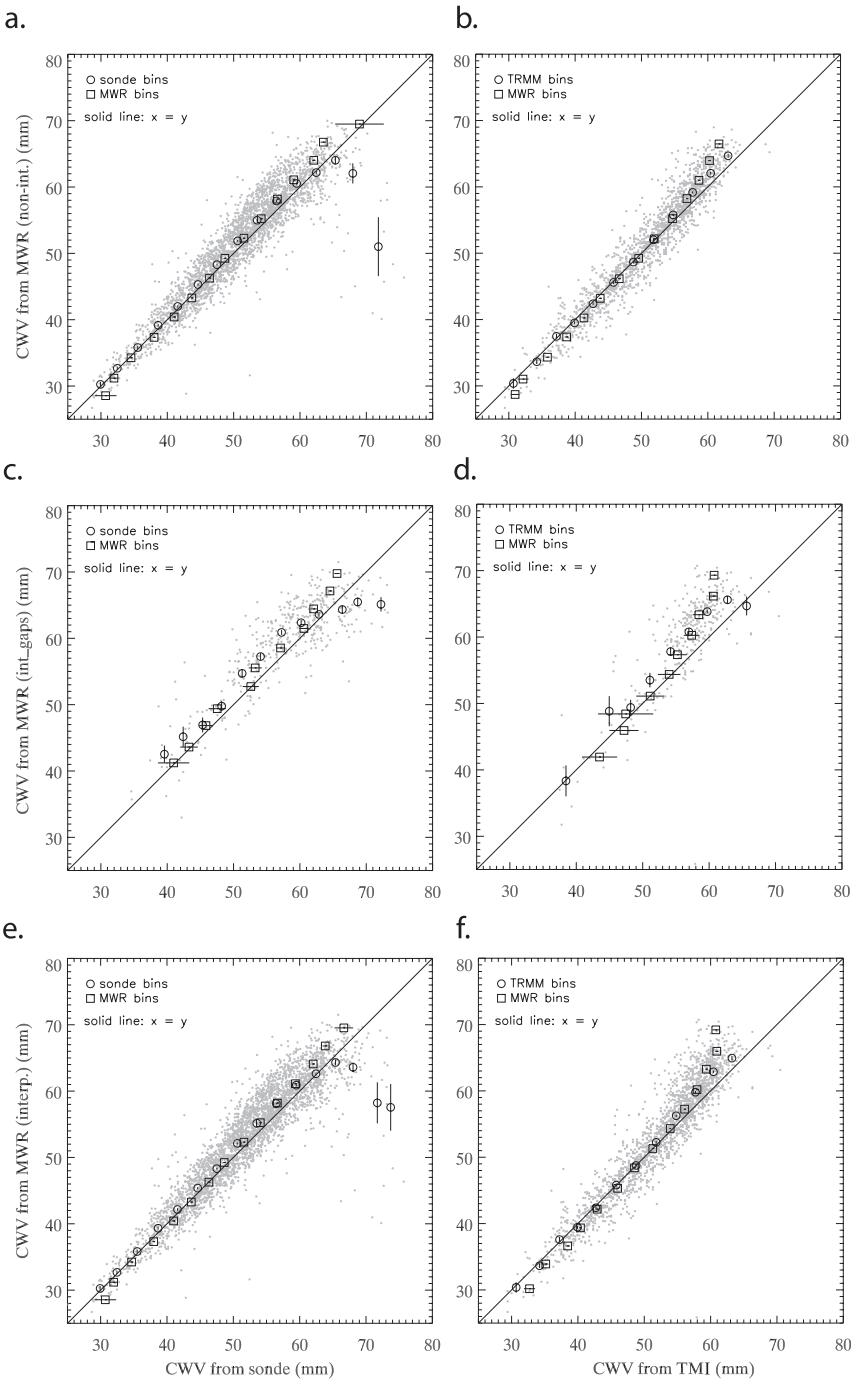

FIG. 4. Conditional averages and associated standard errors of column water vapor values for MWR vs sondes and vs TMI (with scatterplots in background), for (a),(b) non-gap-filled MWR data, (c),(d) only the filled gaps in the MWR data, and (e),(f) full interpolated MWR data. Conditional averages are performed (binned) on each variable in turn. Bins are 3 mm wide, and only bins with at least five counts are plotted.

events). The relatively long, gradual approach to higher CWV values (as compared with the narrow peaks of CLW and precipitation) stands out and is consistent with the autocorrelation scales shown in Fig. 1.

The gradual CWV rise from long-term mean conditions, labeled "synoptic-scale increase," starts about 36 h before the precipitation peak and lasts about 30 h. If we assume advection by a mean wind of 10 m s^{-1}, this

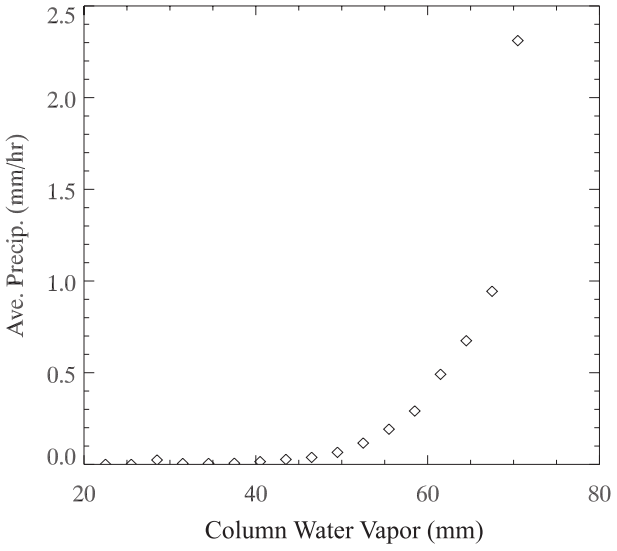

FIG. 5. Precipitation conditioned on CWV 3 h earlier, with 3-h bin width. Bins with fewer than 1000 counts are excluded.

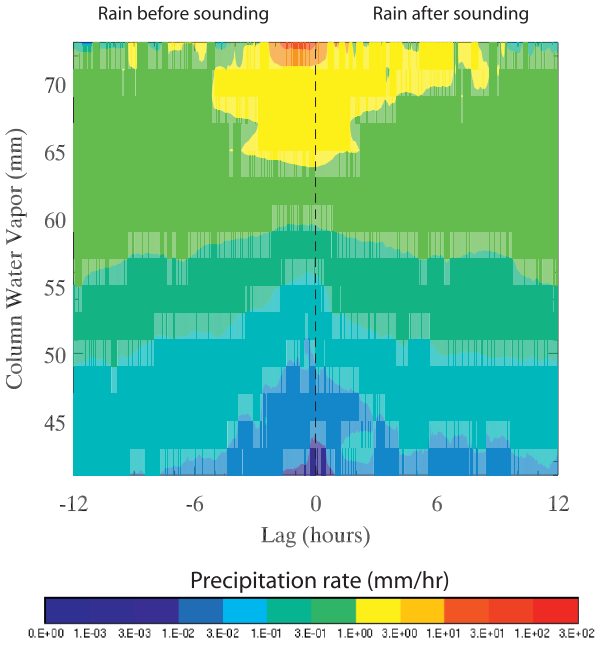

FIG. 6. Precipitation rate conditioned on gap-filled column water vapor at various leads or lags. Lag axis measures time after CWV measurement (i.e., CWV leads rainfall on the right side of the diagram).

translates to a spatial scale of almost 1200 km. In contrast, about 7 h before the peak there is a much steeper increase in CWV. This seems to be a separate ''mesoscale'' feature (whose corresponding spatial scale by the same estimation would be about 250 km), which is larger than both the precipitation increase (deep convective element) and the CLW increase. The existence of such a feature suggests a role of CWV, and therefore lower-free-tropospheric moisture (Holloway and Neelin 2009), in mesoscale convective organization, consistent with the positive moisture–convection feedback found in many previous studies (e.g., Parsons et al. 2000; Tompkins 2001; Grabowski 2003; Derbyshire et al. 2004; Bretherton et al. 2005). Specific mechanisms potentially explaining this feature include the initial upward motion of a gravity wave propagating ahead of a convective system with top-heavy heating (e.g., Nicholls et al. 1991; Mapes 1993; Liu and Moncrieff 2004; Fovell et al. 2006) and a ''mesolow'' (cf. Houze 2004).

In the CLW composite, there seems to be a somewhat slower decrease after the peak than an increase before it. This delayed decrease is labeled ''trailing mesoscale cloud'' and can also be seen in the precipitation composite. Based on composites of stratiform clouds (not shown), it appears that this is mainly related to convective clouds originating from below 2 km, although it is possible that clouds with midlevel bases are not being adequately measured. Composites of cloud-top height are discussed below. The asymmetric CLW and precipitation peak could suggest a hysteresis in the system—once a threshold is crossed, for instance in CWV, the system tends to rain for a while, perhaps because of the positive feedbacks between CWV and deep convection discussed above. Another possible explanation is that precipitation maxima may be preferentially located toward the leading edge of mesoscale convective systems propagating over Nauru.

Figure 7 indicates that the synoptic-scale rise before the precipitation event is fairly slow and constant, whereas the corresponding decline afterward, while perhaps delayed by a few hours, is somewhat steeper, resulting in values at 24-h lag that are lower than the values at −24 h. This provides additional support for the view that high CWV conditions are created by factors substantially separated from precipitation and deep convection. A different proposed mechanism for slow CWV rise during relatively suppressed conditions such as a dry intrusion (Numaguti et al. 1995; Mapes and Zuidema 1996; Brown and Zhang 1997; DeMott and Rutledge 1998; Parsons et al. 2000)—namely, that shallow cumuli form and then evaporate into the free troposphere—is not immediately apparent from the CLW composite. However, it may be that the presence of average CLW over an extended time helps increase lower-free-tropospheric moisture, and thus CWV, without showing up as an increase in CLW.

To further explore the idea of transitions between different cloud regimes associated with the temporal changes of column water vapor, we have also composited

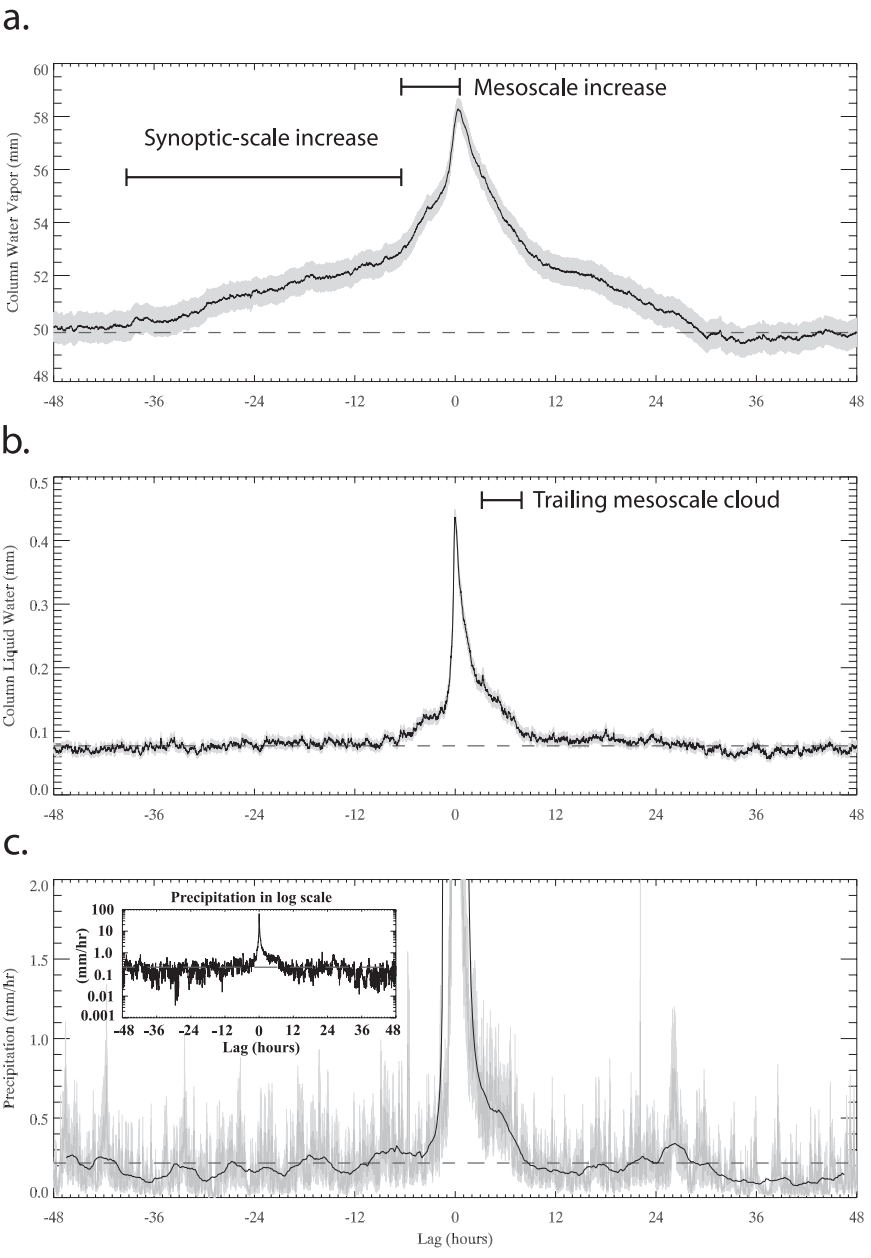

FIG. 7. (a) Gap-filled CWV, (b) gap-filled CLW, and (c) precipitation rate, composited on locally high (above 0.97 mm h^{-1}) precipitation events for ±48-h lags (330 events). Light gray shading shows ±1 standard error. Dark gray shading in (c) shows actual composites each minute; the black line is a 3-h running mean. Dashed lines are long-term means. Labels indicate periods for which interpretations are discussed in the text.

several measures of cloud-top height and cloud-base height on the same precipitation events as in Fig. 7. The first composite, shown in Fig. 8a, is that of the median of convective cloud-top height, where convective cloud is defined as any cloud with the cloud base below 2 km (note that the black lines show 3-h running means for all panels of Fig. 8). The median is chosen to minimize the effects of attenuation during heavy rainfall, which tends to reduce the very high cloud-top heights near zero lag. Interestingly, the convective clouds stay relatively high up to around 7 h after the peak precipitation, corresponding to the trailing mesoscale cloud seen in Figs. 7b,c. The convective cloud fraction is fairly symmetric around zero lag (Fig. 8b), but when this is divided into convective clouds reaching above and below 5 km (Fig. 8c) the low convective cloud fraction goes from slightly

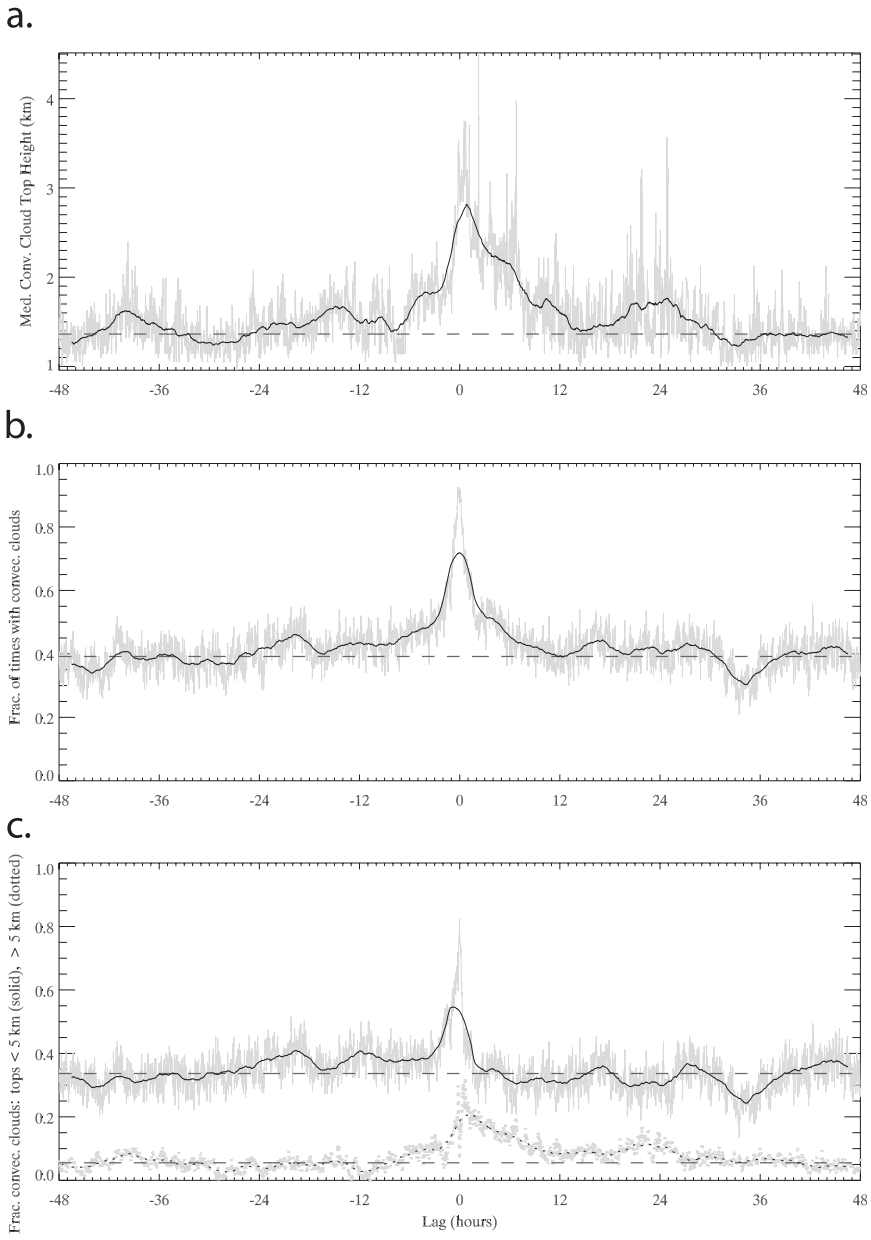

FIG. 8. (a) Median convective cloud-top height and (b) fraction of event times with convective clouds. (c) As in (b), but divided further by cloud top above (dotted) or below 5 km (solid), composited as in Fig. 7 on locally high precipitation events. Gray shading shows actual composites each minute; black lines are 3-h running means; dashed lines are long-term means.

above the ambient levels at about −24-h lag to a brief peak at zero lag before returning to near-ambient levels at about 4 h; the high convective cloud fraction stays above the ambient level from about −8 to 27 h. Finally, in an attempt to separate stratiform-type clouds from deep convective clouds, we also composited fractions of only those high, thick clouds that have cloud-base height greater than 5 km and cloud top above 8 km (not shown), but these are also fairly symmetric about zero lag, rising from about 10% ambient mean to around 15%–20% for ±12-h lag. Although there may be some difficulties using this dataset to discern multiple cloud levels during rainfall, these data indicate that it is mainly deep and midlevel convective cloud that trail after the maximum precipitation rather than upper-level stratiform cloud.

Another question that can be addressed with these data is the relationship between CWV and the transition

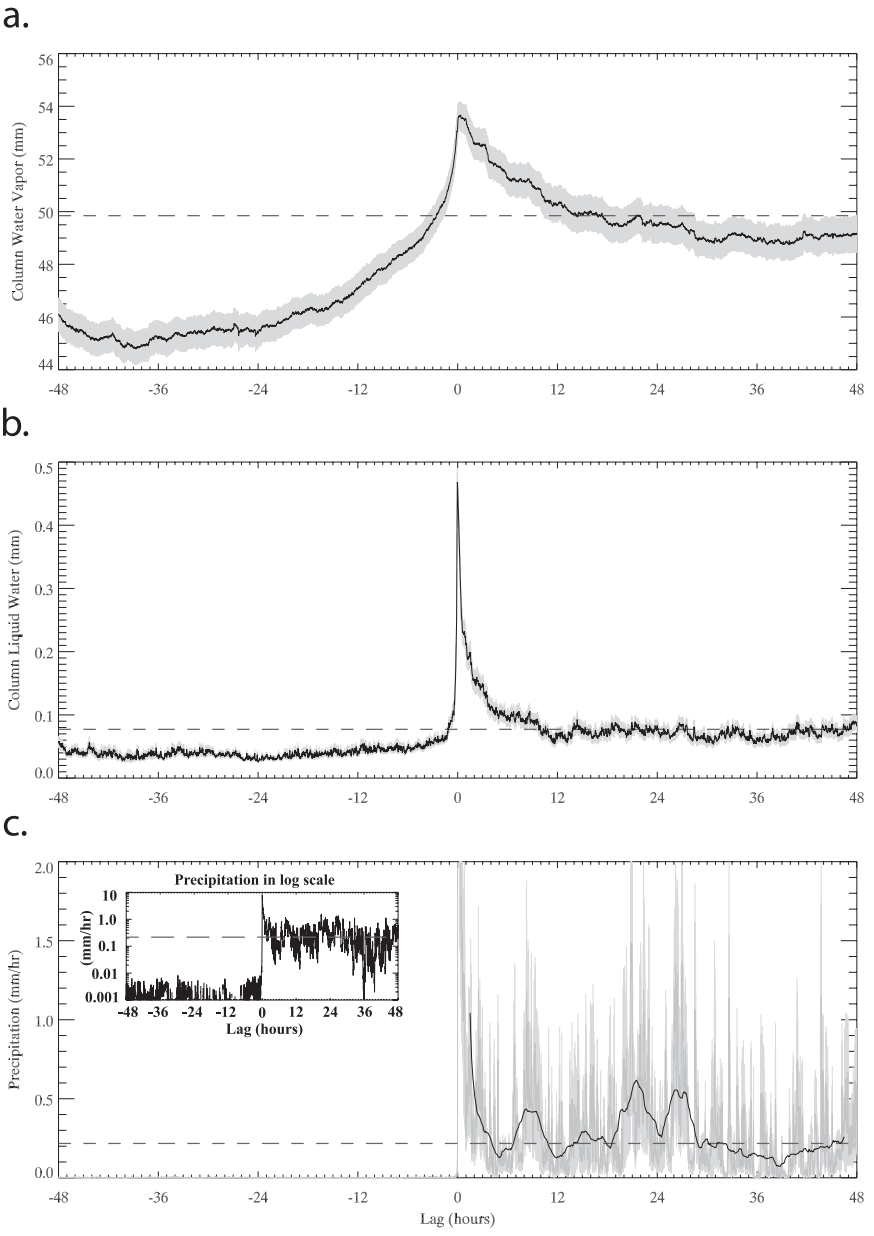

FIG. 9. (a) Gap-filled CWV, (b) gap-filled CLW, and (c) precipitation rate, composited on the ends of 48-h low-precipitation (below 0.97 mm h^{-1}) periods for ±2-day lags (184 events). Light gray shading shows ±1 standard error. Dark gray shading in (c) shows actual composites each minute; black line is a 3-h running mean; dashed lines are long-term means.

from suppressed convection to more normal conditions. Figure 9 shows composites made on the beginning of events larger than the median positive precipitation rate (0.97 mm h^{-1}) and preceded by periods below that rate lasting at least 48 h (184 events). These figures show that even in the absence of significant rain at Nauru, there is a rise of CWV preceding the return to normal rainfall. The CWV and CLW values before precipitation are lower than normal in Fig. 9, with higher levels afterward corresponding to wetter conditions (the nonsmoothed peak at zero lag, inset at log scale, reaches 7.9 mm h^{-1}). Between around −36 and −12 h, there is a slow increase in CWV of approximately 2 mm, fairly consistent with that seen in Fig. 7a. After −12 h or so, the increase accelerates, increasing over 5 mm between about −6- and 0-h lag. The latter steep increase is also consistent with Fig. 7a and could be associated with the involvement of mesoscale processes on top of the synoptic-scale background.

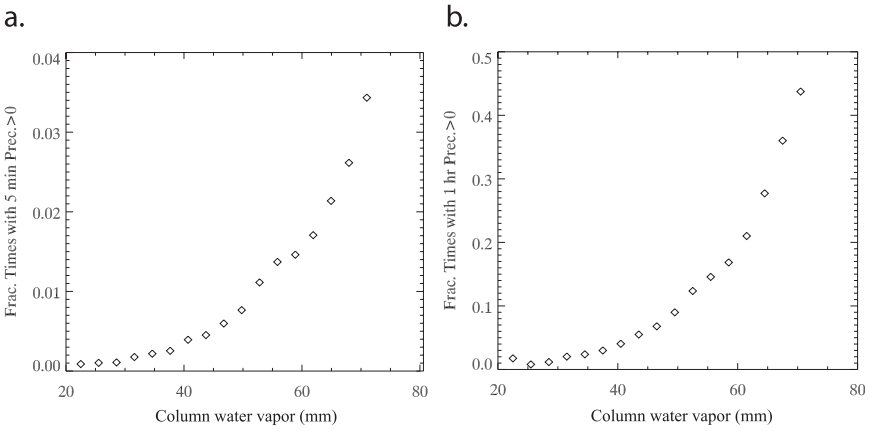

FIG. 10. Fractional probability of positive precipitation, given no initial precipitation, in the next (a) 5 min and (b) 1 h. These are conditionally averaged on non-gap-filled column water vapor 1 min earlier at 3-mm bin width. Bins with fewer than 1000 counts are excluded.

6. Transition probabilities

To further investigate the relationship between CWV and transitions to rainfall, we have conditioned probabilities of rain on both CWV and precipitation. Figure 10 shows the probability of precipitation during the subsequent 5 min or 1 h after a given CWV value using non-gap-filled data, conditioned on there being no rain at the time of the CWV measurement. In other words, the figure shows the probability of transition from no rain to rain as a function of CWV. This conditional probability exhibits a pickup at high CWV similar to the pickup of the mean precipitation (although the mean precipitation also has a contribution from an increase in the expected value of the precipitation given that it is raining). These probabilities are not very high for the water vapor values that most commonly occur. Hourly probabilities rise to not quite 45% even at high values (69–72 mm) of CWV. At still high but more common values of CWV, around 54 mm, the probability of rain in a given hour is less than 15%. Thus, as CWV rises, there will typically be a lag before the rain begins, which should average a couple of hours long—for instance, using an hourly precipitation probability of 15% typical of CWV around 55 mm, and an independence assumption, the probability of *no* rain in two hours is $(1 - 0.15)^2 = 72\%$. For the highest CWV bin, 43% precipitation probability yields a probability of no rain in two hours of over 30%.

The independence assumption should only be used to give rough estimates. As a check, using the probabilities based on the 5-min data in Fig. 10a, the probability of having no rain for one hour with initial CWV at 69–72 mm is 65%, somewhat higher than the correct value of 57% (taking 1 minus the 1-h rain probability at that CWV value in Fig. 10b). We also note that the wet-window problem (see section 2) can affect the estimated probabilities slightly (using gap-filled data, not shown, gives slightly larger estimated probabilities).

This conditional probability is similar to a statistic that one might use in a stochastic convection scheme: the probability of launching a convective element, for a given state of the water vapor (and temperature), given that the grid cell is not yet convecting. The measurement here is an imperfect analog because it is for the initiation of precipitation, and we do not know precisely the spatial area to which this probability corresponds. Nonetheless, it provides motivation for revising parameterization assumptions that initiate deep convection and precipitation deterministically and immediately upon reaching a certain state of temperature and moisture.

The precipitation probability without conditioning on zero precipitation at time zero also shows a similar shape pickup to the curves in Fig. 10. The lag behavior of this probability (Fig. 11) has a similar pattern to that of the mean precipitation pickup at many lags and leads (see discussion of Fig. 6 above).

7. Periods of high column water vapor

The probabilities in Fig. 10 demonstrate that even at relatively high CWV values the chance of rainfall, given no initial rain, is still significantly below 100%. This makes it instructive to look at high CWV times and see how precipitation behaves in those times. Another question that arises from the above analyses is whether the CWV increase and the precipitation pickup at high enough CWV are actually sharper than they appear from composites and averages. We may be smoothing these increases by averaging over many different sharp increases that occur at different lags.

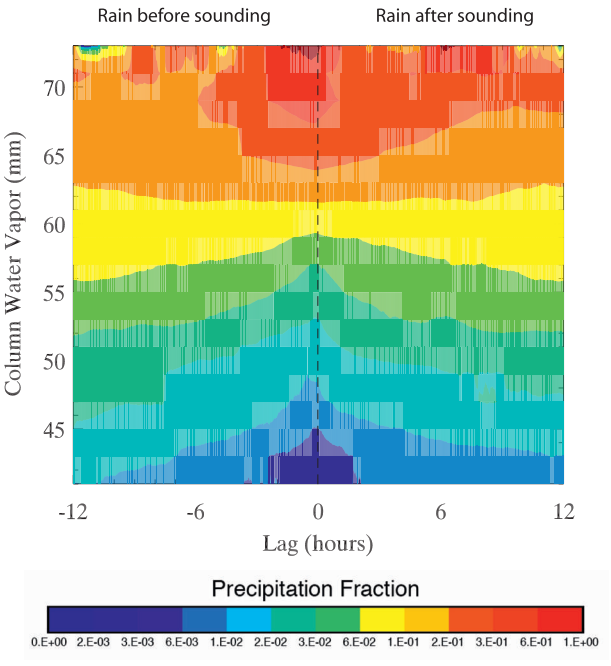

FIG. 11. Fraction of positive precipitation conditionally averaged on gap-filled column water vapor at various leads/lags. Lag axis measures time after CWV measurement (i.e., CWV leads rainfall on the right side of the diagram).

To investigate these points, we composite CWV, CLW, and precipitation rate on locally high CWV. However, we then center our composite window not on these maxima, but on the crossing point from below to above 54 mm CWV that precedes and occurs closest to the maxima in each case (even if this is up to two weeks before the beginning of the initial time window used to identify maxima). We choose 54 mm because it is near the base of the sharp increase seen in Fig. 7a and near the center of the transition to high precipitation probability in Fig. 10.

These composites, which include 304 events, are shown in Fig. 12. Note that there is indeed a rather sharp increase of precipitation rate and an even more pronounced sharp increase in CLW, in addition to the sharp increase in CWV that is partly a product of the compositing method. The values of CLW and precipitation respond immediately, although the increases are relatively small compared with those in Fig. 7, in which composites are centered on the relatively narrow deep convective peaks.

To measure this effect further, we composite precipitation rate over one hour starting at the first precipitation at or following the transition to 54-mm CWV (zero lag in Fig. 12), excluding events with missing values (291 events total). This composite, shown in the inset of Fig. 12c, shows higher maximum values than in the main composite of Fig. 12c, as expected—there is fairly large variability in the start time for precipitation, with a median of 1.95 h, a mean of 5.83 h, and an interquartile distance of 3.13 h (as shown by the vertical bars and caret in Fig. 12a). In addition, 5% of the events had already started at zero lag, and these are counted as having zero start time. Since the median start time is about 2 h, this gives a probability of *not* raining in this time of 50%. We can compare this to the probability of no rain in the next hour (given no rain at time zero) in Fig. 10b, which is about 0.8 at 54 mm CWV—for two hours, the probability drops to $0.8^2 = 0.64$, which is fairly consistent. Also, the precipitation rate composited over these different events peaks near the beginning, as expected from the compositing criteria, but remains fairly high throughout the period, suggesting that, once started, many events last an hour or more.

8. Conclusions

Analysis of eight years of 1-min resolution microwave radiometer and optical gauge data at Nauru Island is used to explain the temporal relationships between column water vapor (CWV) and precipitation. Nauru Island is used because of the unique instrumental record; however, our findings are believed to be relevant to the tropics in general, especially in oceanic regions. High CWV is associated with a strong pickup of precipitation even 10–12 h in the future. CWV is found to have large autocorrelation times compared with column liquid water (CLW) and precipitation, which helps explain how CWV can have skill in predicting precipitation probability. In composites on strong precipitation events, CWV slowly rises starting about 36 h before the event peak, well before there are increases in average precipitation or CLW, suggesting that there is some synoptic-scale cause of increased CWV.

CWV increase is not simply a result of local rainfall moistening its immediate surroundings, but there are strong indications of involvement of mesoscale dynamics in the increase to the highest values of CWV associated with strong precipitation. Specifically, in the composites on strong precipitation events, beginning around 7 h prior to the event there is a much sharper CWV peak, which is likely associated with mesoscale convective events. This supports arguments (Mapes 1993; Grabowski and Moncrieff 2004) that the interaction between convective cells, via free tropospheric moistening and thus higher CWV, can create a positive moisture–convection feedback that allows for organization of convection on larger scales. The rainfall and CLW are distributed asymmetrically around zero lag, with the trailing increased precipitation being associated with more convective clouds

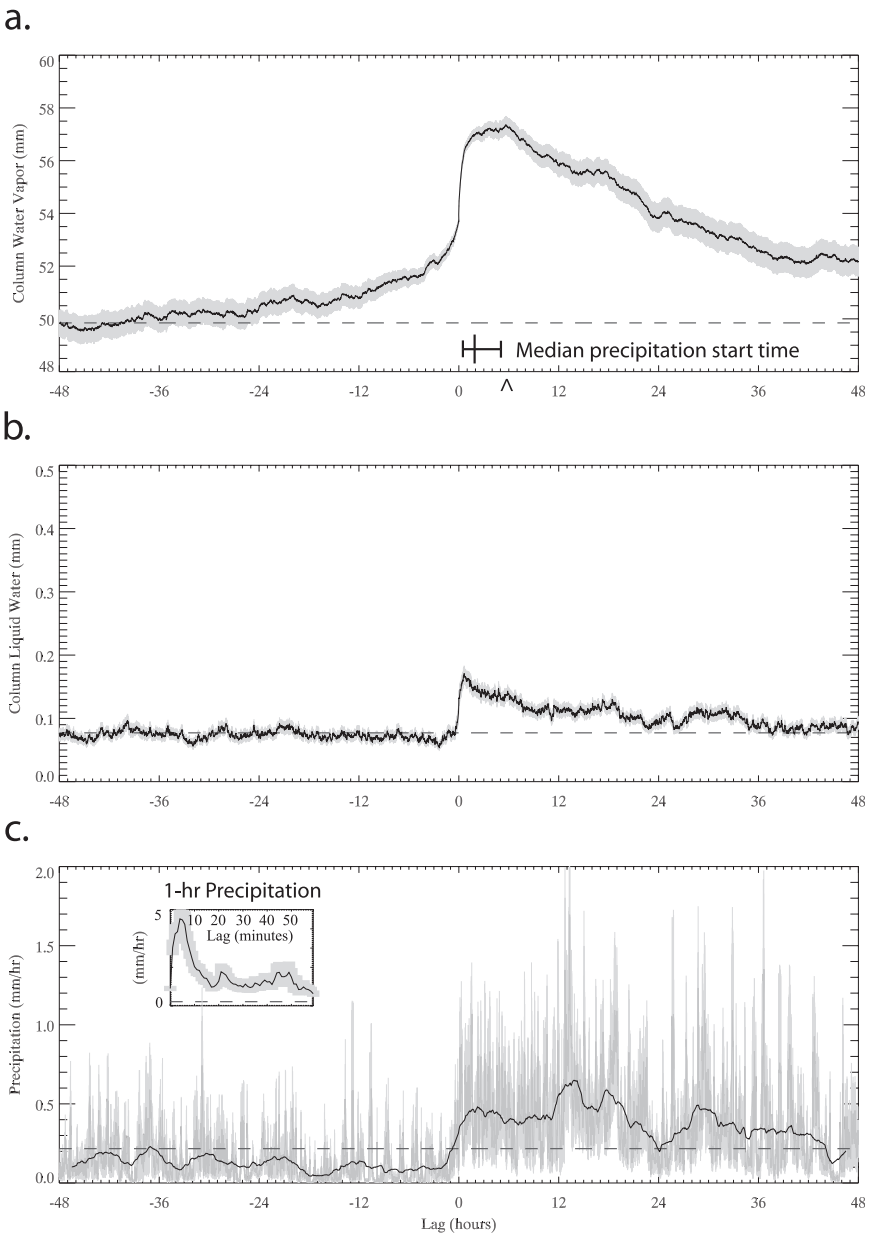

FIG. 12. (a) Gap-filled CWV, (b) gap-filled CLW, and (c) precipitation rate, composited on locally high CWV (above 54 mm and largest value within ±48 h), but centered on the last value below 54-mm CWV before the maximum (304 events). Inset shows 1-h precipitation event composites (see text). In (a), median and first and third quartiles (vertical bars at 1.95, 0.63, and 5.08 h, respectively), as well as the mean (caret mark at 5.83 h), of event start times are shown.

originating from the boundary layer and reaching above 5 km in height.

CWV also tends to increase ahead of the termination of suppressed precipitation conditions. This increase exhibits slow ''synoptic-scale'' and faster ''mesoscale'' components similar to those in the composites on precipitation maxima. Furthermore, composites on increases in CWV show that they do indeed accompany significant increases in cloudiness and precipitation, and that the precipitation increase can occur with a range of lags, averaging several hours, after the CWV increase.

Even in periods of high CWV, probabilities of initial precipitation in a 5-min period remain low enough that there tends to be a lag before the start of the next precipitation event. High CWV, then, can be thought of as a suitable predictor variable for precipitation. This framework

suggests applications to the stochastic prediction of precipitation in models; however, a model incorporating such a scheme would also require the accurate simulation of processes such as free-tropospheric moistening by convection and the advection of dry intrusions from the subtropics in order to predict CWV.

Acknowledgments. This work was supported in part by National Science Foundation Grant ATM-0645200 and National Oceanic and Atmospheric Administration Grant NA08OAR4310882. JDN acknowledges the John Simon Guggenheim Memorial Foundation and the National Center for Atmospheric Research for sabbatical support. CEH was supported in part by NASA Earth System Science Fellowship Grant NNX06AF83H and in part by a UCLA Dissertation Year Fellowship. ARM data were used with the cooperation of the U.S. Department of Energy as part of the Atmospheric Radiation Measurement Program Climate Research Facility. We thank M. Cadeddu, M. Moncrieff, O. Peters, and B. Stevens for helpful discussions and K. Hales-Garcia for TMI data processing.

REFERENCES

Bretherton, C. S., M. E. Peters, and L. E. Back, 2004: Relationships between water vapor path and precipitation over the tropical oceans. *J. Climate,* **17,** 1517–1528.

——, P. N. Blossey, and M. Khairoutdinov, 2005: An energy-balance analysis of deep convective self-aggregation above uniform SST. *J. Atmos. Sci.,* **62,** 4273–4292.

Brown, R. G., and C. Zhang, 1997: Variability of midtropospheric moisture and its effect on cloud-top height distribution during TOGA COARE. *J. Atmos. Sci.,* **54,** 2760–2774.

Clothiaux, E. E., T. P. Ackerman, G. G. Mace, K. P. Moran, R. T. Marchand, M. A. Miller, and B. E. Martner, 2000: Objective determination of cloud heights and radar reflectivities using a combination of active remote sensors at the ARM CART sites. *J. Appl. Meteor.,* **39,** 645–665.

DeMott, C. A., and S. Rutledge, 1998: The vertical structure of TOGA COARE convection. Part II: Modulating influences and implications for diabatic heating. *J. Atmos. Sci.,* **55,** 2748–2762.

Derbyshire, S. H., I. Beau, P. Bechtold, J.-Y. Grandpeix, J.-M. Piriou, J.-L. Redelsperger, and P. M. M. Soares, 2004: Sensitivity of moist convection to environmental humidity. *Quart. J. Roy. Meteor. Soc.,* **130,** 3055–3079.

Fovell, R. G., G. L. Mullendore, and S. H. Kim, 2006: Discrete propagation in numerically simulated nocturnal squall lines. *Mon. Wea. Rev.,* **134,** 3735–3752.

Grabowski, W. W., 2003: MJO-like coherent structures: Sensitivity simulations using the cloud-resolving convection parameterization (CRCP). *J. Atmos. Sci.,* **60,** 847–864.

——, and M. W. Moncrieff, 2004: Moisture-convection feedback in the tropics. *Quart. J. Roy. Meteor. Soc.,* **130,** 3081–3104.

Haertel, P. T., and G. N. Kiladis, 2004: Dynamics of 2-day equatorial waves. *J. Atmos. Sci.,* **61,** 2707–2721.

Hilburn, K. A., and F. J. Wentz, 2008: Intercalibrated passive microwave rain products from the unified microwave ocean retrieval algorithm (UMORA). *J. Appl. Meteor. Climatol.,* **47,** 778–794.

Holloway, C. E., and J. D. Neelin, 2009: Moisture vertical structure, column water vapor, and tropical deep convection. *J. Atmos. Sci.,* **66,** 1665–1683.

Houze, R. A., Jr., 2004: Mesoscale convective systems. *Rev. Geophys.,* **42,** RG4003, doi:10.1029/2004RG000150.

Jensen, M. P., and A. D. Del Genio, 2006: Factors limiting convective cloud-top height at the ARM Nauru Island Climate Research Facility. *J. Climate,* **19,** 2105–2117.

Kiladis, G. N., K. H. Straub, and P. T. Haertel, 2005: Zonal and vertical structure of the Madden–Julian oscillation. *J. Atmos. Sci.,* **62,** 2790–2809.

Liljegren, J., S.-A. Boukabara, K. Cady-Pereira, and S. Clough, 2005: The effect of the half-width of the 22-GHz water vapor line on retrievals of temperature and water vapor profiles with a 12-channel microwave radiometer. *IEEE Trans. Geosci. Remote Sens.,* **43,** 1102–1108, doi:10.1109/TGRS.2004.839593.

Liu, C., and M. W. Moncrieff, 2004: Effects of convectively generated gravity waves and rotation on the organization of convection. *J. Atmos. Sci.,* **61,** 2218–2227.

Maloney, E. D., and D. L. Hartmann, 1998: Frictional moisture convergence in a composite life cycle of the Madden–Julian oscillation. *J. Climate,* **11,** 2387–2403.

Mapes, B. E., 1993: Gregarious tropical convection. *J. Atmos. Sci.,* **50,** 2026–2037.

——, and P. Zuidema, 1996: Radiative–dynamical consequences of dry tongues in the tropical troposphere. *J. Atmos. Sci.,* **53,** 620–638.

——, S. Tulich, J. Lin, and P. Zuidema, 2006: The mesoscale convection life cycle: Building block or prototype for large-scale tropical waves? *Dyn. Atmos. Oceans,* **42,** 3–29.

——, R. Milliff, and J. Morzel, 2009: Composite life cycle of maritime tropical mesoscale convective systems in scatterometer and microwave satellite observations. *J. Atmos. Sci.,* **66,** 199–208.

Mather, J. H., T. P. Ackerman, W. E. Clements, F. J. Barnes, M. D. Ivey, L. D. Hatfield, and R. M. Reynolds, 1998: An atmospheric radiation and cloud station in the tropical western Pacific. *Bull. Amer. Meteor. Soc.,* **79,** 627–642.

Neelin, J. D., O. Peters, J. W.-B. Lin, K. Hales, and C. E. Holloway, 2008: Rethinking convective quasi-equilibrium: Observational constraints for stochastic convective schemes in climate models. *Philos. Trans. Roy. Soc. London,* **366A,** 2579–2602, doi:10.1098/rsta.2008.0056.

——, ——, and K. Hales, 2009: The transition to strong convection. *J. Atmos. Sci.,* **66,** 2367–2384.

Nicholls, M. E., R. A. Pielke, and R. W. Cotton, 1991: Thermally forced gravity waves in an atmosphere at rest. *J. Atmos. Sci.,* **48,** 1869–1884.

Numaguti, A., R. Oki, K. Nakamura, K. Tsuboki, N. Misawa, T. Asai, and Y.-M. Kodama, 1995: 4–5-day-period variation on low-level dry air observed in the equatorial western Pacific during the TOGA COARE IOP. *J. Meteor. Soc. Japan,* **73,** 267–290.

Parsons, D. B., K. Yoneyama, and J.-L. Redelsperger, 2000: The evolution of the tropical western Pacific atmosphere–ocean system following the arrival of a dry intrusion. *Quart. J. Roy. Meteor. Soc.,* **126,** 517–548.

Peters, O., and J. D. Neelin, 2006: Critical phenomena in atmospheric precipitation. *Nat. Phys.,* **2,** 393–396.

Sherwood, S. C., 1999: Convective precursors and predictability in the tropical western Pacific. *Mon. Wea. Rev.,* **127,** 2977–2991.

——, and R. Wahrlich, 1999: Observed evolution of tropical deep convective events and their environment. *Mon. Wea. Rev.,* **127,** 1777–1795.

——, P. Minnis, and M. McGill, 2004: Deep convective cloud-top heights and their thermodynamic control during CRYSTAL-FACE. *J. Geophys. Res.,* **109,** D20119, doi:10.1029/2004JD004811.

Sobel, A. H., S. E. Yuter, C. S. Bretherton, and G. N. Kiladis, 2004: Large-scale meteorology and deep convection during TRMM KWAJEX. *Mon. Wea. Rev.,* **132,** 422–444.

Stokes, G. M., and S. E. Schwartz, 1994: The Atmospheric Radiation Measurement (ARM) Program: Programmatic background and design of the cloud and radiation test bed. *Bull. Amer. Meteor. Soc.,* **75,** 1201–1221.

Tian, B., D. E. Waliser, E. J. Fetzer, B. H. Lambrigtsen, Y. L. Yung, and B. Wang, 2006: Vertical moist thermodynamic structure and spatial–temporal evolution of the MJO in AIRS observations. *J. Atmos. Sci.,* **63,** 2462–2485.

Tompkins, A. M., 2001: Organization of tropical convection in low vertical wind shears: The role of water vapor. *J. Atmos. Sci.,* **58,** 529–545.

Westwater, E. R., B. B. Stankov, D. Cimini, Y. Han, J. A. Shaw, B. M. Lesht, and C. N. Long, 2003: Radiosonde humidity soundings and microwave radiometers during Nauru99. *J. Atmos. Oceanic Technol.,* **20,** 953–971.

Zelinka, M. D., and D. L. Hartmann, 2009: Response of humidity and clouds to tropical deep convection. *J. Climate,* **22,** 2389–2404.